

The alignment of the polarization of Herbig Ae/Be stars with the interstellar magnetic field¹

Cláudia V. Rodrigues², Marília J. Sartori³, Jane Gregorio-Hetem⁴, A. Mário Magalhães⁴

ABSTRACT

We present a study of the correlation between the direction of the symmetry axis of the circumstellar material around intermediate mass young stellar objects and that of the interstellar magnetic field. We use CCD polarimetric data on 100 Herbig Ae/Be stars. A large number of them shows intrinsic polarization, which indicates that their circumstellar envelopes are not spherical. The interstellar magnetic field direction is estimated from the polarization of field stars. There is an alignment between the position angle of the Herbig Ae/Be star polarization and that of the field stars for the most polarized objects. This may be an evidence that the ambient interstellar magnetic field plays a role in shaping the circumstellar material around young stars of intermediate mass and/or in defining their angular momentum axis.

Subject headings: stars: pre-main sequence — ISM: magnetic fields — polarization

1. Introduction

The role of the magnetic field in the star formation processes is a longstanding problem in astrophysics. The magnetic field is proposed to act in the support of molecular clouds against the gravitational force by some authors (e.g., Mouschovias & Ciolek 1999). A different view is

²Instituto Nacional de Pesquisas Espaciais/MCT – Av. dos Astronautas, 1758 – 12227-010 - São José dos Campos - SP – Brazil; claudiavr@das.inpe.br

³Laboratório Nacional de Astrofísica/MCT – 37504-364 - Itajubá - MG - Brazil

⁴Instituto de Astronomia, Geofísica e Ciências Atmosféricas/Un. São Paulo – R. do Matão, 1225 – 05508-900 - São Paulo - SP – Brazil

¹Based on observations made at the Observatório do Pico dos Dias, Brazil, operated by the Laboratório Nacional de Astrofísica.

that these clouds are not stable and exist as ephemeral structures. In this case, the turbulence drives the interstellar medium large scale structure (e.g., McKee & Ostriker 2007). It is possible to address this issue by the search of evidences about the importance of interstellar magnetic field in the star forming process. From an observational point of view, many works have searched for a correlation between the direction of the interstellar magnetic field and the geometry of young stellar objects (YSOs) traced by disk axis, outflow direction, or observed polarization. We cite two of them. Tamura & Sato (1989) have found a correlation between the interstellar magnetic field direction and the infrared polarization angle in a sample of 47 YSOs in Taurus-Auriga molecular cloud. This sample is dominated by T Tauri stars. Recently, Ménard & Duchêne (2004) have studied 37 T Tauri stars in the same region and found no correlation between the local magnetic field and the geometry of the YSOs.

Herbig Ae/Be objects (HAeBe) are pre-main sequence stars, analogue to T Tauri stars, but of intermediate mass. Lists of HAeBe stars can be found in the compilation of Thé et al. (1994) and in The Pico dos Dias Survey (PDS), a search for T Tauri stars based on IRAS colors (Gregorio-Hetem et al. 1992; Torres et al. 1995). In spite of the focus on low mass YSOs, PDS has also found around a hundred of HAeBe candidates (Vieira et al. 2003; Torres 1999). In this work, we revisited the issue of alignment of the interstellar magnetic field with the YSO geometry using a large sample of HAeBe objects. The study of the polarization in the context of the circumstellar material properties will be done elsewhere (Sartori M. et al., in preparation). In Section 2, we describe the acquisition and reduction of the polarimetric data and the technique to calculate the interstellar and intrinsic stellar polarization. The results and discussion are presented in Section 3. In the last section, we summarize our findings.

2. Observations

We obtained polarimetric data on 102 fields containing probable HAeBe stars selected from Thé et al. (1994), Torres (1999), and Vieira et al. (2003). The observations were done with the 0.60-m Boller & Chivens telescope at the Observatório do Pico dos Dias, Brazil, operated by the Laboratório Nacional de Astrofísica, Brazil, from 1998 to 2002. We used a CCD camera modified by the polarimetric module described in Magalhães et al. (1996). The used detector is a SiTe back-illuminated CCD, 1024×1024 pixels. This combination of telescope and instrumentation results in a field-of-view of $10'5 \times 10'5$ (1 pixel = $0'62$). The data were taken using a V filter. We have collected eight images of each field. Table 1 lists the observation date and the integration time (for one image) for each field. The

reduction followed the standard steps of differential photometry using the IRAF facility² and the package PCCDPACK (Pereyra 2000; Pereyra & Magalhães 2002). Polarized standard stars were observed to convert the instrumental position angle to the equatorial reference frame. Unpolarized standard star measurements were consistent with zero within the errors and hence no corrections for instrumental polarization were applied to the data. Measurements using a Glan filter, which provide the efficiency of the instrument, indicate that no correction is needed considering the instrumental precision. The observed polarization data are presented in Table 1. It contains the 102 program stars plus 2 confirmed post-AGB that contaminate the PDS sample and are not included in the analysis.

The observed polarization of a YSO is usually composed by two components: an intrinsic polarization plus an interstellar polarization component. The intrinsic component is produced by the scattering of the central source emission off the circumstellar material. In the path from the object to the observer, the interstellar medium introduces a foreground polarization. These two polarizations are combined vectorially to produce the observed polarization. Hence, to obtain the intrinsic polarization one must estimate the foreground value to be subtracted from the observed polarization.

The striking majority of stars in the sky is either intrinsically unpolarized or has small, uncorrelated intrinsic polarization. The stellar field is hence dominated by objects presenting only the interstellar component. For our purposes we may then estimate the foreground polarization towards the object of interest by a weighted average of the polarization of the field stars with a good signal-to-noise ratio ($P > 3\sigma_P$). The average was done from the Stokes parameters Q and U. The number of objects in each of our fields vary from 3 to more than 1000. Such a high number of field objects having angular distances to the HAeBe smaller than 5' gives us confidence that this technique to estimate the interstellar component is reliable. It is also probably statistically better than the estimates in previous works in which the foreground objects are located angularly farther from the YSO and in smaller numbers due to the use of photomultiplier as the detector.

The foreground and intrinsic polarizations, as well as the number of field objects used in the estimate of the interstellar polarization, are shown in Table 1. The polarization of each foreground star for each field will be available as a Vizier catalog as well as the polarization vectors superposed on an optical image. Two objects, HD 23302 and HD 23480, are too bright and there is no other object in the image with sufficient signal-to-noise to enable an estimate to the foreground polarization. These two objects are not included in the following

²IRAF is distributed by National Optical Astronomy Observatories, which is operated by the Association of Universities for Research in Astronomy, Inc., under contract with the National Science Foundation.

analysis. Our final sample analysis is therefore composed by 100 objects.

3. Results and discussion

The interstellar polarization is caused by aligned aspherical grains that produce the dichroism of the interstellar medium. The alignment mechanism is not yet completely understood. The classical mechanism is based on paramagnetic dissipation by rotating grains with superparamagnetic inclusions (Davis & Greenstein 1951; Jones & Spitzer 1967). However, this mechanism may be not efficient enough. Recently, a promising mechanism based on radiative torques has been proposed (Lazarian & Hoang 2007). In both cases, however, the direction of the magnetic field projected in the plane of the sky can be traced by the position angle of the optical interstellar polarization. A recent review on grain alignment can be found at Lazarian (2007).

The intrinsic polarization position angle is related to the axis of symmetry of the HAeBe envelope. It depends on many factors but we can say in a simple way that in optically thin envelope the polarization is parallel to symmetry axis, and in optically thick case it is perpendicular. A proper understanding of this issue is obtained by the modelling of the scattering of the central source light in the YSO circumstellar material (e.g., Brown & McLean 1977; Bastien & Menard 1990; Whitney & Hartmann 1993).

Is the geometry of HAeBe stars in our sample related to the direction of the interstellar magnetic field? We try to answer such a question by checking whether the position angles of the intrinsic polarization and the surrounding interstellar polarization are correlated. For this purpose, we define $\Delta\theta$ as the difference between the intrinsic and foreground polarization directions. $\Delta\theta$ runs from 0 to 90° .

Figure 1 (solid line) shows the cumulative histogram of $\Delta\theta$ for the 100 objects of our sample. The dotted straight line represents the behavior of an uniform distribution. To compare quantitatively both distributions, we used the Kuiper statistic (e.g., Paltani 2004). It is a modification of the Kolmogorov-Smirnov test and is appropriate for cyclic quantities such as $\Delta\theta$. Figure 1 shows that the sample as a whole is obviously not uniform. Indeed, the resulting Kuiper statistic has a probability of only 1.3%, so the hypothesis that our observed distribution is uniform can be discarded. In addition, as the observed curve stays *below* that of the uniform distribution, it means that $\Delta\theta$ concentrates around 90° .

An inspection of the data shows that this behavior is caused by objects with small values of *observed* polarization. In this case, the intrinsic polarization has the same modulus as the foreground polarization but is perpendicular to it; this causes the concentration of $\Delta\theta$ near

90°. This probably arises as a result of two factors. The HAeBe object may be nearer to us than most of the field stars. In that case, the foreground polarization must be negligible and the observed polarization should have not been corrected by a foreground component. In addition, if the *real* intrinsic polarization is undetected given the errors, our estimate of the intrinsic polarization is wrong: it simply reflects the foreground polarization rotated by 90°. We may add that a situation in which the interstellar polarization would be perpendicular and have the same modulus of the intrinsic component is less likely. As a result of this discussion, the concentration of $\Delta\theta$ around 90° may carry an observational bias.

To circumvent such problems, we also built the cumulative histogram considering only objects having the observed polarization larger than 3% (Figure 1, dot-dashed line): these are 19 in number. These objects are less affected by the foreground correction, since they must have a larger contribution from the intrinsic polarization to the observed value. In addition, the polarization in all these cases has a high signal-to-noise ratio and hence a well determined interstellar component. In this sample, the Kuiper statistic for $\Delta\theta$ has a probability smaller than 2%. Using (the 27) objects with polarization larger than 2% (Figure 1, dashed line), the statistic has this same probability. We also note that, as shown in Figure 1, these two samples now present $\Delta\theta$ clustered around zero.

Star forming regions are dense portions of the ISM. Consequently they usually present high values of interstellar extinction and polarization. Because of that, we have also checked whether the above results might be biased by cases in which the observed polarization is dominated by the interstellar component. Figure 1 (short dash - long dash line) shows the cumulative distribution considering the objects with the observed polarization larger than 3% and the intrinsic polarization larger than 2% (16 objects), a sub-sample that excludes cases where the interstellar component is the predominant one. This constraint does not modify significantly the histogram and the resulting Kuiper statistic has a probability smaller than 12%.

We concluded that the observed distribution of $\Delta\theta$ for the sub-sample of objects presenting high signal-to-noise measurements and reliable values of intrinsic polarization is non uniform with a clear excess of objects with $\Delta\theta$ around zero. This result suggests that the polarization of HAeBe stars has a tendency to be aligned with the ambient interstellar magnetic field. It can be interpreted as an indication that the magnetic field of the material that collapsed to form the star can play a role in defining the YSO geometry and/or the symmetry axis of the envelope.

Our findings contrast with the work of Ménard & Duchêne (2004) which does not show an alignment between the YSO axis and the interstellar magnetic field using a sample of T Tauri stars. However, previous works, using samples of less evolved objects, indicate an

alignment (Kobayashi et al. 1978; Dyck & Lonsdale 1979; Heckert & Zeilik 1981; Hodapp 1984; Cohen et al. 1984; Strom & Strom 1987). A possible solution for this discrepancy is that the alignment may be more easily traced in the less evolved, low mass YSO. This occurs because, during its slow pre-main sequence evolution, an object can move away from its birth place or present a rotation of its axis direction. From a point of view of the YSO mass, HAeBe stars evolve faster than T Tauri stars, which could make the observation of the alignment more probable in the higher mass group. We note that in our sample objects with P greater than 3% also have larger mid-infrared excess (Sartori et al., in preparation), putting these objects in an early evolutionary stage.

Some observational arguments have been recently put forward in favor of a fossil origin of the magnetic fields in Ap/Bp stars (e.g., Wade et al. 2009). This hypothesis assumes that the interstellar magnetic field present in the cloud that originates the star is amplified along the star evolution and is present in the main sequence stage. This is another piece of evidence that the formed (proto)stellar object can have a memory of the interstellar magnetic field of the parent cloud and its direction, as indicated by our results.

4. Conclusions

We present the results of optical CCD polarimetry of a sample of 102 fields containing HAeBe stars. The direction of the intrinsic polarization of the YSO, and hence their envelope axis, shows a correlation with interstellar magnetic field direction for the sample as a whole. This result may be an observational bias, as discussed in the text. Sub-samples of the more polarized objects present a statistically significant tendency to have the YSO polarization aligned with the interstellar magnetic field. This indicates that the geometry of HAeBe objects retained a memory of the interstellar magnetic field.

We acknowledge the use of the NASA’s Astrophysics Data System Service and the SIMBAD database, operated at CDS, Strasbourg, France. This work was partially supported by Fapesp (CVR and AMM: Proc. 2001/12589-1; JGH: Procs. 2001/09018-2 and 2005/00397-1) and CNPq (AMM).

This is an author-created, un-copyedited version of an article accepted for publication in The Astrophysical Journal. IOP Publishing Ltd is not responsible for any errors or omissions in this version of the manuscript or any version derived from it.

Facilities: LNA:BC0.6m ()

REFERENCES

- Bastien, P., & Menard, F. 1990, *ApJ*, 364, 232
- Brown, J. C., & McLean, I. S. 1977, *A&A*, 57, 141
- Cohen, R. J., Rowland, P. R., & Blair, M. M. 1984, *MNRAS*, 210, 425
- Davis, L. & Greenstein, J. L. 1951, *ApJ*, 114, 206
- Dyck, H. M., & Lonsdale, C. J. 1979, *AJ*, 84, 1339
- Gregorio-Hetem, J., Lepine, J. R. D., Quast, G. R., Torres, C. A. O., & de La Reza, R. 1992, *AJ*, 103, 549
- Heckert, P. A., & Zeilik, M., II 1981, *AJ*, 86, 1076
- Hodapp, K.-W. 1984, *A&A*, 141, 255
- Jones, R. V., & Spitzer, L. J. 1967, *ApJ*, 147, 943
- Kobayashi, Y., Kawara, K., Maihara, T., Okuda, H., Sato, S., & Noguchi, K. 1978, *PASJ*, 30, 377
- Lazarian, A. 2007, *Journal of Quantitative Spectroscopy and Radiative Transfer*, 106, 225
- Lazarian, A., & Hoang, T. 2007, *MNRAS*, 378, 910
- Magalhães, A. M., Rodrigues, C. V., Margoniner, V. E., Pereyra, A., & Heathcote, S., 1996, in *ASP Conf. Ser. 97, Polarimetry of the Interstellar Medium*, Eds. W. G. Roberge & D. C. B. Whittet (San Francisco:ASP), 118
- McKee, C. F., & Ostriker, E. C. 2007, *ARA&A*, 45, 565
- Ménard, F., & Duchêne, G. 2004, *A&A*, 425, 973
- Mouschovias, T. C., & Ciolek, G. E. 1999, *NATO ASIC Proc. 540: The Origin of Stars and Planetary Systems*, 305
- Paltani, S. 2004, *A&A*, 420, 789
- Pereyra, A., 2000. *Dust and Magnetic Fields in Dense Regions of the Interstellar Medium*, PhD Thesis, Univ. São Paulo
- Pereyra, A., & Magalhães, A. M. 2002, *ApJS*, 141, 469

- Strom, S. E., & Strom, K. M. 1987, *Star Forming Regions*, 115, 255
- Tamura, M., & Sato, S. 1989, *AJ*, 98, 1368
- Thé, P. S., de Winter, D., & Perez, M. R. 1994, *A&AS*, 104, 315
- Torres, C. A. O. 1999, *Special Publ. 10* (Rio de Janeiro Observatrio Nacional)
- Torres, C. A. O., Quast, G., de La Reza, R., Gregorio-Hetem, J., & Lépine, J. R. D. 1995, *AJ*, 109, 2146
- Vieira, S. L. A., Corradi, W. J. B., Alencar, S. H. P., Mendes, L. T. S., Torres, C. A. O., Quast, G. R., Guimarães, M. M., & da Silva, L. 2003, *AJ*, 126, 2971
- Wade, G. A., Alecian, E., Grunhut, J., Catala, C., Bagnulo, S., Folsom, C. P., & Landstreet, J. D. 2009, [arXiv:0901.0347](https://arxiv.org/abs/0901.0347)
- Whitney, B. A., & Hartmann, L. 1993, *ApJ*, 402, 605

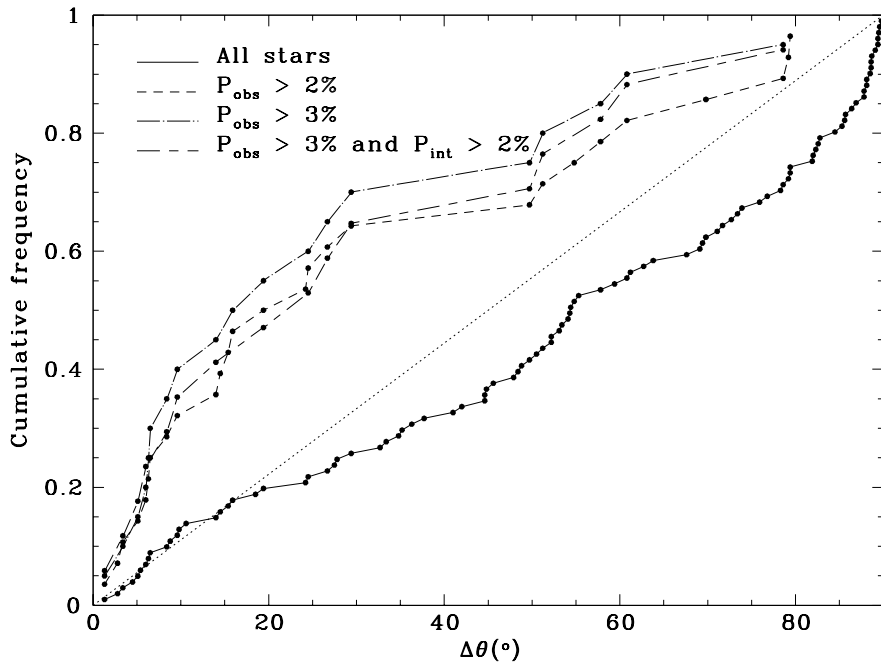


Fig. 1.— Cumulative frequency distributions of the difference between the intrinsic and interstellar polarization angle, $\Delta\theta$, for our H A e Be sample and sub-samples. See text for details.

Table 1. Polarimetry of HAeBe objects

Object	V ¹ (mag)	Exposure (s)	UT Date	Observed			# of objects	Foreground			Intrinsic			Ref. ²
				P (%)	σ_P (%)	PA (deg)		P (%)	σ_P (%)	PA (deg)	P (%)	σ_P (%)	PA (deg)	
PDS 002	10.9	100	1998 Nov 25	0.128	0.045	135.4	12	0.190	0.022	107.0	0.161	0.050	176.1	1
PDS 004	10.7	120	1998 Nov 25	1.018	0.033	45.8	48	0.557	0.020	49.8	0.473	0.039	41.0	1
HD 23302 ³	3.7	5	1999 Jul 28	0.238	0.038	113.8	0	-	-	-	-	-	-	3
HD 23480 ³	4.2	7	1999 Jul 28	0.507	0.033	141.2	0	-	-	-	-	-	-	3
PDS 168	17.3	300	1999 Jul 29	8.377	0.278	62.0	33	2.544	0.015	62.9	5.835	0.278	61.6	1
PDS 172	7.6	30	1998 Nov 24	0.354	0.013	52.1	30	0.126	0.070	127.8	0.469	0.071	48.4	1,2
PDS 176	9.8	100	1998 Nov 24	0.141	0.021	64.4	33	0.173	0.019	17.6	0.230	0.028	88.7	1,2
PDS 110	10.4	200	1998 Nov 24	0.366	0.066	27.6	21	0.367	0.024	117.9	0.733	0.070	27.7	3
PDS 178	7.8	25	1998 Nov 24	0.120	0.021	140.6	14	2.369	0.094	83.3	2.421	0.096	172.0	1
PDS 179	9.7	90	1998 Nov 25	0.336	0.027	80.0	61	0.260	0.015	87.8	0.111	0.031	60.3	1
PDS 180	10.1	120	1999 Apr 08	0.266	0.026	58.9	25	0.188	0.011	90.6	0.248	0.028	37.5	1,2
PDS 114	10.0	90	1998 Nov 25	0.161	0.032	35.5	89	0.060	0.022	10.5	0.131	0.039	45.7	1
PDS 184	10.1	120	1999 Apr 08	0.421	0.017	118.5	65	0.616	0.013	122.4	0.207	0.021	40.4	1
PDS 183	8.3	30	1998 Nov 24	0.368	0.011	41.9	21	1.849	0.084	88.1	1.900	0.085	3.6	1,2
PDS 185	6.5	2	2002 Oct 19	0.455	0.043	179.0	22	0.972	0.099	168.8	0.568	0.108	70.7	1
PDS 190	9.3	90	1998 Nov 25	0.390	0.149	75.5	20	0.319	0.071	104.1	0.345	0.165	50.0	1
PDS 191	8.9	40	1999 Apr 08	0.173	0.007	75.4	5	0.153	0.011	41.4	0.183	0.013	100.8	1,2
PDS 192	9.9	40	2002 Oct 19	0.359	0.026	46.8	93	0.081	0.033	18.1	0.323	0.042	52.9	1
PDS 193	13.9	400	1998 Nov 25	2.183	0.114	86.3	9	0.087	0.057	17.2	2.249	0.127	87.0	1,2
PDS 194	9.8	100	1999 Apr 08	0.300	0.023	31.1	6	2.035	0.304	123.9	2.334	0.305	33.5	1,2
PDS 016	9.0	40	1998 Nov 24	0.269	0.036	12.3	29	0.227	0.033	176.4	0.142	0.049	41.0	1
PDS 201	8.9	50	1998 Nov 24	0.573	0.037	58.4	41	0.202	0.011	35.0	0.459	0.039	67.7	1
PDS 019	13.9	200	1999 Apr 08	0.274	0.033	129.0	37	0.259	0.013	109.9	0.175	0.035	162.1	1
PDS 020	10.6	90	1998 Nov 25	0.571	0.032	165.7	146	1.171	0.011	161.1	0.614	0.034	66.8	1
PDS 021	10.4	100	1998 Nov 25	1.598	0.022	29.7	41	0.738	0.013	32.6	0.867	0.026	27.2	1
PDS 022	10.2	100	1998 Nov 25	0.201	0.018	102.0	82	0.083	0.010	134.6	0.182	0.021	89.8	1
PDS 225	6.9	2	1999 Apr 11	0.974	0.044	26.3	15	0.681	0.219	172.7	0.948	0.223	47.0	1
HD 51585	11.1	80	1999 Apr 11	0.522	0.045	43.3	207	0.183	0.018	12.5	0.464	0.048	53.5	3
PDS 241	12.1	120	1999 Apr 11	3.672	0.037	104.8	315	0.324	0.009	127.4	3.451	0.038	102.9	1
PDS 249	14.2	300	1999 Apr 08	1.703	0.190	54.6	204	0.545	0.007	147.1	2.246	0.190	55.2	1
PDS 272	9.8	40	1999 Jan 22	0.130	0.026	109.6	129	0.183	0.019	83.1	0.147	0.032	150.7	1
PDS 277	10.0	45	1999 Jan 22	0.040	0.049	97.0	178	0.537	0.014	51.2	0.540	0.051	139.0	1

Table 1—Continued

Object	V ¹ (mag)	Exposure (s)	UT Date	Observed				Foreground			Intrinsic			Ref. ²
				<i>P</i> (%)	σ_P (%)	<i>PA</i> (deg)	# of objects	<i>P</i> (%)	σ_P (%)	<i>PA</i> (deg)	<i>P</i> (%)	σ_P (%)	<i>PA</i> (deg)	
PDS 031	8.5	8	1999 Apr 11	0.138	0.043	82.1	77	0.687	0.035	87.8	0.552	0.055	179.2	1
HBC 563	14.2	200	1999 Jan 22	3.307	0.241	177.7	54	0.067	0.021	26.6	3.272	0.242	177.2	2
PDS 033	12.3	80	1999 Jan 22	0.862	0.071	76.7	82	0.034	0.025	121.1	0.862	0.075	75.5	1
PDS 034	14.0	400	1999 Jan 23	2.799	0.418	117.6	229	0.515	0.006	104.9	2.344	0.418	120.3	1
HD 76534	8.0	10	1999 Apr 11	0.466	0.017	127.4	29	2.813	0.041	76.3	2.947	0.044	161.9	2
PDS 281	8.9	24	1999 Jan 23	1.375	0.039	160.2	28	0.067	0.032	106.2	1.397	0.050	161.5	1
PDS 286	12.2	250	1999 Jan 18	8.217	0.060	171.8	58	1.623	0.019	178.5	6.649	0.063	170.1	1
PDS 290	14.5	300	1999 Apr 11	2.408	0.227	149.8	234	0.669	0.012	147.8	1.741	0.227	150.6	1
GSC 8593-2802	12.0	300	1999 Jan 22	1.946	0.058	115.8	448	1.146	0.007	132.8	1.184	0.058	99.4	1
HD 85567	8.6	14	1999 Jan 21	0.478	0.035	105.7	174	0.715	0.035	116.1	0.317	0.049	42.2	2
PDS 303	9.3	25	1999 Jan 21	0.579	0.044	125.3	273	0.587	0.018	116.8	0.173	0.048	167.3	1
PDS 037	13.5	300	1999 Jan 18	3.253	0.104	120.1	217	0.530	0.010	131.9	2.775	0.104	117.9	1
PDS 315	10.9	80	1999 Jan 21	2.141	0.034	158.6	681	0.931	0.007	173.3	1.406	0.035	149.1	1
GSC 8618-2363	12.0	300	1999 Apr 08	1.493	0.070	64.9	352	0.703	0.004	128.5	1.998	0.070	56.8	1
HD 94509	9.1	120	1999 Apr 08	0.688	0.015	123.1	322	0.480	0.007	143.1	0.445	0.017	101.1	2
HD 95881	8.3	10	1999 Jan 21	1.504	0.034	116.2	81	1.500	0.021	122.6	0.335	0.040	74.7	2
PDS 327	8.5	12	1999 Jan 21	0.613	0.032	114.0	276	0.428	0.019	130.4	0.343	0.037	92.7	1
HD 97048	8.5	10	1999 Jan 22	2.519	0.044	143.3	3	3.629	0.066	138.1	1.238	0.079	37.5	2
PDS 339	7.8	7	1999 Jan 21	0.056	0.040	99.9	114	0.261	0.047	95.0	0.206	0.062	3.6	1
PDS 340	6.8	3	1999 Jan 21	0.236	0.039	50.6	24	3.204	0.127	126.0	3.412	0.133	36.9	1,2
PDS 057	9.2	40	1999 Jan 21	0.737	0.027	90.9	488	1.122	0.017	89.3	0.388	0.032	176.2	1,2
PDS 344	13.2	300	1999 Apr 11	1.590	0.053	56.4	304	1.681	0.019	89.4	1.783	0.056	26.7	1
PDS 061	6.6	2	1999 Jan 22	0.032	0.063	167.2	20	1.699	0.086	116.7	1.705	0.107	26.1	1,2
PDS 140	13.1	300	1999 Apr 11	1.852	0.099	89.4	476	0.773	0.008	83.6	1.106	0.099	93.4	1
PDS 353	13.2	480	2000 Jun 21	0.666	0.056	22.5	1034	1.733	0.004	84.1	2.170	0.056	1.5	1
Hen 3-847	10.6	80	1999 Apr 11	0.348	0.035	20.7	186	0.631	0.017	53.0	0.575	0.039	159.6	2
PDS 361	12.9	600	2000 Jun 22	0.219	0.034	1.3	1109	0.398	0.004	97.5	0.614	0.034	5.3	1
PDS 364	13.5	300	1999 Apr 11	2.298	0.030	68.8	411	2.600	0.006	70.3	0.327	0.031	171.1	1
PDS 067	13.5	600	2000 Jun 21	0.768	0.067	7.4	666	2.287	0.004	66.3	2.731	0.067	163.5	1
PDS 069	9.8	60	1999 Feb 12	0.681	0.040	147.0	22	0.245	0.055	112.9	0.632	0.068	157.5	1
HD 130437	10.0	120	1999 Apr 10	5.818	0.085	56.9	20	1.252	0.034	61.6	4.587	0.092	55.6	2
HBC 596	12.8	300	1999 Apr 11	4.198	0.181	46.8	115	1.482	0.015	59.8	2.939	0.182	40.4	2

Table 1—Continued

Object	V ¹ (mag)	Exposure (s)	UT Date	Observed				Foreground			Intrinsic			Ref. ²
				<i>P</i> (%)	σ_P (%)	<i>PA</i> (deg)	# of objects	<i>P</i> (%)	σ_P (%)	<i>PA</i> (deg)	<i>P</i> (%)	σ_P (%)	<i>PA</i> (deg)	
HD 132947	8.9	15	1999 Apr 07	1.254	0.042	56.1	62	1.293	0.016	59.9	0.173	0.045	6.5	2
PDS 389	14.2	300	1999 Jul 28	4.630	0.218	133.4	54	0.708	0.018	56.4	5.275	0.219	135.0	1
PDS 394	13.5	300	1999 Jul 27	2.235	0.166	15.0	312	1.448	0.010	50.9	2.252	0.166	176.1	1
PDS 395	8.4	10	1999 Apr 07	0.062	0.110	147.6	100	1.755	0.099	43.1	1.808	0.148	133.7	1
PDS 144	12.8	300	1999 Apr 10	4.653	0.070	124.1	108	0.759	0.013	116.0	3.930	0.071	125.6	1
PDS 398	7.1	3	1999 Nov 07	0.680	0.027	86.7	9	2.665	0.090	82.4	1.995	0.094	170.9	1,2
PDS 399	8.6	15	1999 Apr 10	1.705	0.022	61.0	385	1.553	0.018	54.9	0.378	0.028	91.2	1
PDS 076	8.7	10	1999 Apr 07	0.803	0.039	81.5	20	0.077	0.027	85.6	0.727	0.047	81.1	1,2
PDS 406	13.9	300	1999 Apr 10	4.719	0.081	33.6	348	2.049	0.009	17.1	3.201	0.081	43.8	1
PDS 078	8.2	10	1999 Apr 07	0.367	0.059	14.5	65	0.455	0.047	16.4	0.092	0.075	114.1	1,2
HD 144668	7.0	6	1999 Apr 08	0.579	0.019	166.5	7	0.498	0.010	5.6	0.361	0.021	137.2	2
PDS 080	9.1	14	1999 Apr 07	0.039	0.052	45.8	47	0.589	0.059	4.9	0.585	0.079	93.0	1
PDS 415	12.0	200	1999 Apr 08	1.418	0.022	28.5	59	1.536	0.019	29.7	0.133	0.029	132.9	1
Hen 3-1191	13.7	300	1999 Apr 10	5.885	0.146	46.0	546	0.752	0.006	43.0	5.138	0.146	46.4	2
HD 150193	8.9	15	1999 Apr 07	4.780	0.108	56.7	34	4.330	0.057	56.1	0.460	0.122	62.4	2
PDS 431	13.4	300	1999 Jul 28	1.276	0.175	38.4	222	1.086	0.007	35.3	0.229	0.175	53.8	1
V921 Sco	11.4	80	1999 Apr 07	2.509	0.256	114.7	133	1.343	0.016	121.7	1.249	0.256	107.2	2
KK Oph	11.9 ⁴	45	1999 Apr 10	3.426	0.092	169.6	62	0.913	0.063	33.3	3.505	0.112	162.1	2
PDS 453	12.9	200	1999 Apr 07	3.608	0.060	48.9	412	2.635	0.021	7.3	4.208	0.064	68.1	1
PDS 095	11.0	100	1999 Apr 11	1.634	0.096	34.3	70	1.041	0.022	165.6	2.048	0.098	49.4	1
PDS 096	11.0	100	1999 Apr 11	1.662	0.031	175.3	95	1.329	0.011	177.5	0.352	0.033	166.9	1
PDS 465 ⁵	12.9	300	1999 Apr 11	9.152	0.251	43.4	501	1.298	0.009	48.3	7.876	0.251	42.6	1
PDS 469	12.8	300	1999 Apr 11	1.315	0.031	72.4	637	1.739	0.007	62.7	0.663	0.032	132.1	1
PDS 473	6.9	4	1999 Apr 08	0.417	0.035	36.0	63	1.140	0.063	42.5	0.740	0.072	136.1	1,2
PDS 477	14.4	300	1999 Jul 28	1.188	0.090	24.8	196	0.900	0.012	66.1	1.395	0.091	4.9	1
PDS 514	8.2	12	1999 Apr 08	0.095	0.029	105.2	125	0.892	0.024	100.6	0.798	0.038	10.1	1
PDS 518	12.2	300	1999 Jul 28	1.816	0.040	93.6	4	3.051	0.089	43.7	3.807	0.098	119.6	1,2
VV Ser	11.6 ⁴	400	2000 Jun 21	1.780	0.043	77.5	5	1.566	0.079	54.5	1.322	0.090	106.7	2
MWC 300	10.5	300	2000 Jun 21	4.843	0.035	58.2	265	4.001	0.012	55.2	0.960	0.037	71.1	2
PDS 520	14.7	300	1999 Jul 28	3.513	0.107	15.2	9	0.391	0.029	70.1	3.664	0.111	12.3	1
HBC 284/1	12.5	360	2000 Jun 22	0.916	0.095	67.1	501	0.637	0.009	56.8	0.390	0.095	84.6	2
HBC 284/2	12.5	360	2000 Jun 22	0.691	0.114	72.6	501	0.637	0.009	56.8	0.365	0.114	105.6	2

Table 1—Continued

Object	V ¹ (mag)	Exposure (s)	UT Date	Observed				Foreground			Intrinsic			Ref. ²
				P (%)	σ_P (%)	PA (deg)	# of objects	P (%)	σ_P (%)	PA (deg)	P (%)	σ_P (%)	PA (deg)	
PDS 530	14.0	300	1999 Jul 28	12.305	0.650	55.4	186	1.262	0.019	50.8	11.061	0.650	55.9	1
PDS 543	12.5	360	2000 Jun 21	1.105	0.025	136.8	35	0.610	0.029	175.4	1.138	0.038	121.0	1
PDS 545	8.8	18	1999 Apr 08	3.036	0.025	78.6	44	1.129	0.036	74.5	1.925	0.044	81.0	1
PDS 551	16.6	600	2000 Jun 22	10.930	0.629	117.7	30	0.468	0.029	69.2	10.997	0.630	118.9	1
PDS 564	7.4	4	1999 Apr 08	0.481	0.034	103.7	43	0.471	0.080	4.4	0.939	0.087	99.1	1,2
WW Vul	10.5	100	2000 Jun 21	0.849	0.070	151.3	336	2.065	0.011	12.2	2.118	0.071	113.9	2
PDS 581 ⁵	11.7	80	1999 Apr 07	12.427	0.145	44.4	772	0.326	0.008	69.5	12.221	0.145	43.8	1
HD 190073	7.8	10	1998 Nov 25	0.377	0.026	94.5	15	0.439	0.054	97.9	0.079	0.060	25.2	2

¹Magnitudes are from Torres (1999) or SIMBAD.

²The references of the last column are: (1) Vieira et al. (2003); (2) Thé et al. (1994); (3) Torres (1999).

³The images of the field containing HD23302 and HD23480 do not include objects with signal high enough to estimate the foreground polarization.

⁴B band magnitude.

⁵PDS465 and PDS581 are post-AGB objects.